Journal of the Meteorological Society of Japan, Vol. 95, No. 4, pp. 261−281, 2017
DOI:10.2151/jmsj.2017-015

Coordinated Observation and Numerical Study on a Diurnal Cycle of Tropical Convection over a Complex Topography in West Java, Indonesia

Masanori OIGAWA, Takafumi MATSUDA, Toshitaka TSUDA

Research Institute for Sustainable Humanosphere (RISH), Kyoto University, Kyoto, Japan

and

Noersomadi

Research Institute for Sustainable Humanosphere (RISH), Kyoto University, Kyoto, Japan
National Institute of Aeronautics and Space (LAPAN), Indonesia

(Manuscript received 4 December 2016, in final form 22 April 2017)

Abstract

Mechanisms related to the diurnal cycle of tropical deep convection over a complex terrain were investigated in the Bandung basin, West Java, Indonesia. Observational data were analyzed from X-band radar, Global Navigation Satellite System (GNSS) receivers, and radiosondes, in conjunction with high-resolution numerical model data.

Significant diurnal variation of GNSS-derived precipitable water vapor (PWV), which peaked in the early evening, was observed from 13 to 19 March 2013. During this period, the X-band radar detected convective initiation at approximately 1200 local time over the southern slope of the basin. A 2-km-mesh model successfully simulated the observed diurnal variations of PWV and rainfall from 15 to 17 March 2013. In the model, moist air was present at the bottom of the basin early in the morning, which was transported to the southern slope of the basin by valley wind circulation after sunrise. In contrast, humidity was lower in the northern part of the basin due to a downward circulating valley wind. The valley wind decreased static stability around the southern slope of the basin by transporting moisture. It also caused a low-level wind convergence, resulting in convective initiation on the southern slope of the basin. The GNSS receiver network also recorded this simulated water vapor variability associated with the valley wind.

These results suggest that water vapor in the bottom of the basin during mornings and its advection by the valley wind strongly influences convective initiation in Bandung.

Keywords diurnal variation; complex topography; local circulation; GNSS meteorology; numerical model

Corresponding author: Masanori Oigawa, Research Institute for Sustainable Humanosphere (RISH), Kyoto University, Gokasho, Uji, Kyoto 611-0011, Japan
E-mail: masanori.oigawa@gmail.com
J-stage Advance Published Date: 2 May 2017

1. Introduction

A large number of studies on the diurnal variation of precipitation have been performed in many regions of the world. In the United States, the diurnal variation of precipitation during summer over the region east of the Rocky Mountains and the Great Plains has a strong maximum during midnight and a strong maximum in the late afternoon over the southeastern and western United States (Wallace 1975). Those diurnal cycles are due to not only local circulations and diurnal changes in the frictional drag in the planetary boundary layer but also thermally driven tides in the atmosphere (Dai et al. 1999). Fujibe (1998) described the diurnal variation of precipitation during the warm season in Japan, separating the rainfall event into two types—local precipitation and widespread precipitation. Local precipitation exhibited a pronounced peak between 1500 and 1800 local time (LT) in the inland and between 0300 and 0600 LT at maritime stations. Saito and Kimura (1998) investigated the diurnal variation of convective precipitation in the Chubu-Kanto area, Japan, during summer by using radar data and revealed that the maximum frequency of convective rainfall around mountainous areas occurs during the afternoon, which is earlier than in the plains and coastal sea regions.

In the Maritime Continent, whose diurnal variation of precipitation has also been well investigated, the complex distribution of land and sea and elevated mountains generate local circulations that cause significant variation in the diurnal rainfall. Holland and Keenan (1980) reported the diurnal variation of convection over land areas that was observed by using a geostationary meteorological satellite (GMS). Houze et al. (1981) analyzed the convection over the sea to the north of Borneo using meteorological radar and satellite data. In this area, convection over the sea was typically initiated at midnight by low-level convergence made by land breeze and monsoonal northeasterly flow. Takayabu (2002) analyzed precipitation radar data derived by tropical rainfall measuring mission (TRMM) satellite to investigate diurnal variations of convective and stratiform rain over the equatorial area. It was revealed that the two types of rain vary almost synchronously over the ocean with early morning maximum at 0300–0600 LT. Moreover, over the land, convective rain has a distinct maximum at 1500–1800 LT.

To supplement and extend earlier studies that analyzed GMS and satellite rainfall data, it is necessary to investigate the diurnal cycle of water vapor, which is the energy source of deep convection. Water vapor measurement techniques based on Global Navigation Satellite System (GNSS) meteorology have enabled us to investigate the relationship between the diurnal variation of precipitation and water vapor. GNSS is widely used for the precise determination of the position in a global coordinates. Path length of GNSS radio signals are estimated by measuring the travel time of carrier waves transmitted from GNSS satellites to receiving antennas. However, propagation velocity of radio waves transmitted from a GNSS satellite is delayed in the atmosphere, which can be related to accumulated water vapor amount of the ray path. Dai et al. (2002) investigated the diurnal variation in water vapor over North America using 54 GPS stations and found that the diurnal variation of precipitable water vapor (PWV) peaks around noon in winter and from midafternoon to midnight in summer over most of the central and eastern United States. Iwasaki and Miki (2001) analyzed the diurnal variation of PWV at the "semi-basin" in Japan, which is surrounded by mountains to the east, north, and west, and by the Kanto Plain to the southeast. They showed that a pronounced diurnal variation of PWV with its peak around 1800–2000 LT over the semi-basin was caused by a thermally-induced local circulation. Iwasaki (2004) investigated the relationship between the diurnal variation of PWV and convective activity around Mt. Tanigawa in the northern Kanto District, Japan. The results showed that both PWV and the convective activity exhibited simultaneous maxima. The first peak during the early morning to noon was caused by moisture transport by the valley wind circulation, and the second peak from around 1500 LT to late night was caused by moisture convergence due to the so-called "extended sea breeze" (Kondo 1990), both of which work to reduce the stability of the atmosphere.

Wu et al. (2003) investigated the diurnal variation of moisture, using GNSS-derived PWV data, in a mountainous area of Sumatra Island. The results suggested that moisture transport by local circulation causes large-amplitude diurnal variation of PWV, which reaches its maximum during the late evening. Realini et al. (2014) conducted intensive observations in the Jakarta region using five GNSS receivers, radiosondes, and C-band radar. Intrusions of moisture were detected, originating from the Java Sea, prior to the formation of deep convection in the afternoon. Although PWV is the vertically integrated abundance of water vapor, numerical models can provide a vertical distribution of water vapor. Therefore, this enables us to more easily understand the relationship between the

diurnal variation of rainfall and water vapor (Sato et al. 2003). However, there are a few simulation experiments that use three-dimensional numerical models and compare the model output with GNSS-derived PWV maps. Sato and Kimura (2005) succeeded in reproducing PWV variations caused by valley winds at the central mountains in Japan by using a 5-km-mesh numerical model. Fujita et al. (2011) analyzed PWV variations around the western region offshore of Sumatra reproduced by a 7 km-mesh Nonhydrostatic Icosahedral Atmospheric Model (NICAM).

To investigate the mechanisms of diurnal variation of precipitation over a complex topography, we conducted a coordinated observation campaign in the Bandung basin, West Java, Indonesia, from January to March 2013 (Fig. 1). The altitude of the basin is relatively high (~ 800 m), and the basin is surrounded by volcanic peaks higher than 1500 m above sea level (ASL). The key measuring instruments used in this campaign are seven GNSS receivers, which observed diurnal variations of PWV and its geographical pattern around the basin. An X-band radar was also installed to detect detailed distributions of rain clouds, and radiosondes were launched every 6 h inside the basin. In addition, numerical downscaling experiments were conducted with a horizontal grid interval of 2 km to reproduce the observed diurnal variations. The objective of this study is to investigate the mechanisms of diurnal convection over the complex terrain. This is accomplished by analyzing the intensive observational data in conjunction with high-resolution numerical model data. To the best of the author's knowledge, there have not been any studies that have focused on the diurnal variation of convective activity and water vapor over a complex terrain like Bandung by using intensive observation data and high-resolution numerical models.

The coordinated observation campaign and experimental setup of the numerical model structure are described in Section 2. The analysis and discussion of the results are presented in Sections 3 and 4, respectively. The results of the study are summarized in Section 5.

2. Data and methodology

2.1 Observational campaign from January to March 2013

Three distinct observational campaigns were performed using seven GNSS receivers (Fig. 1b). Observational Period 1 was conducted from 29 January to 5 February 2013, Period 2 was from 10 to 17 February 2013, and Period 3 was from 13 to 19 March 2013. All seven GNSS receiver stations were equipped with an automated weather station (AWS). The GNSS observations were processed using RTNet ver. 3.3.0 software (Rocken et al. 2001). These results were used to estimate the zenith tropospheric delay (ZTD) based on the precise point positioning method (Zumberge

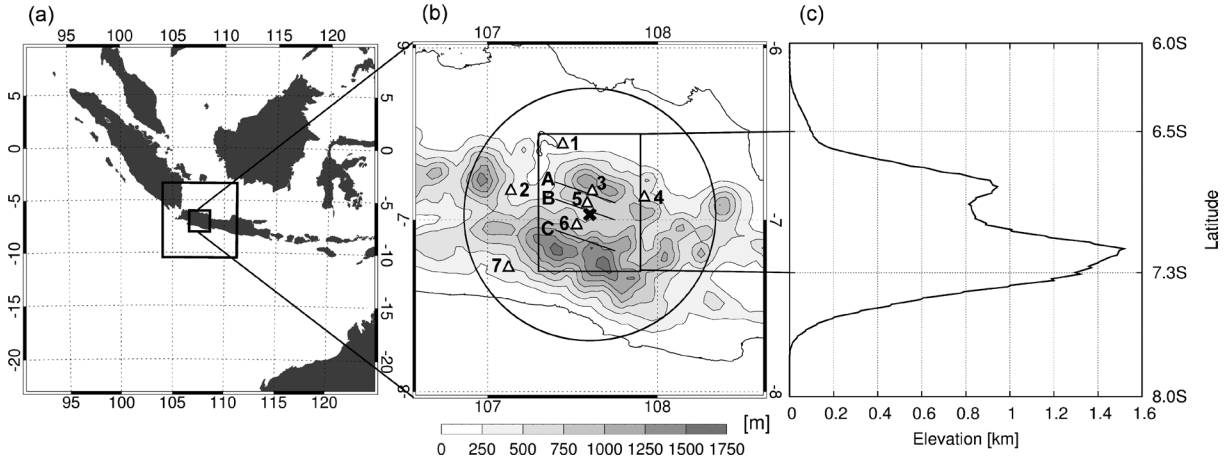

Fig. 1. (a) Domain used for the outer model simulation (15 km grid interval). Large rectangle in this figure indicates a domain used for the inner model simulation (2-km-grid interval). (b) Map of West Java, Indonesia, showing the Bandung basin. GNSS receivers were located at stations 1 to 7 (triangles) during the observational campaign. Radiosondes were launched at station 5 (the LAPAN office). The X-band radar was located at position "X". (c) Latitude section of elevation across the Bandung region, averaged from 107.3 to 107.9°E. In Fig. 10, water vapor distribution is investigated along the three lines in the square.

et al. 1997). Output ZTD data were converted to PWV using surface pressure and temperature data from the AWS. A detailed description of the retrieval of PWV from GNSS can be found in Bevis et al. (1992). The X-band Doppler radar with a horizontal resolution of 250 m was located at 107.692°E 6.975°S at an altitude of 768 m ASL (location X, Fig. 1b). In this study, plan position indicator (PPI) scan data with 5° elevation angle were used for the analysis. The observation range of this scan is shown by a circle in the Fig. 1b. A mean latitudinal elevation profile across the Bandung region is presented in Fig. 1c. Six hourly radiosonde launches were conducted from the LAPAN office (location 5, Fig. 1b). GNSS, radiosonde, and AWS data were collected during all three observational periods. X-band radar observation was only undertaken during Period 3.

2.2 Numerical modeling experiments

To reproduce diurnal variation of precipitation, high-resolution numerical modeling is needed that can express local circulation (Saito et al. 2001; Trilaksono et al. 2011). Numerical downscaling simulations using the Japan Meteorological Agency Nonhydrostatic Model (JMA-NHM) (Saito et al. 2006) were performed to model deep convection during Period 3, when diurnal variation was most distinct with no large-scale disturbance around West Java. An initial numerical simulation was performed to reproduce a large-scale atmospheric condition by using a horizontal grid resolution of 15 km ("15 km-NHM"). The 15 km-NHM had 120 × 120 horizontal grid points and a horizontal domain centered at 6.914°S107.609°E on a Mercator projection. The initial and boundary conditions were derived from JMA global analysis (GANAL) data with a horizontal resolution of 0.1875° × 0.1875° and a time resolution of 6 h (Japan Meteorological Agency 2013). In addition, the 15 km-NHM simulation utilized the Kain–Fritsch cumulus parameterization scheme (Kain and Fritsch 1993) with three-ice bulk microphysics (Lin et al. 1983; Murakami 1990).

The second simulation used a 2 km-mesh model ("2 km-NHM"), which was nested within 15 km-NHM. The 2 km-NHM simulation used three-ice bulk microphysics with no cumulus parameterization. In addition, it had 200 × 200 horizontal grid points and a horizontal domain centered at 6.914°S107.609°E on a Mercator projection. An improved Mellor–Yamada level three scheme (Nakanishi and Niino 2006) was adopted as a turbulent closure model, and a GSM0412 radiation scheme was used (Yabu et al. 2005). A hybrid terrain-following coordinate was adopted as the vertical coordinate. In both models, there were 50 vertical layers, from the surface to the top model level at 21801 m ASL. Layer depth increased upwards in the model, started at 20 m at the lowest level, and increased to 886 m deep in the uppermost level. The prognostic variables were three-dimensional wind components, temperature, pressure, and all water-related quantities such as vapor, rain, clouds, snow, graupel, and ice clouds. The 15 km-NHM (2 km-NHM) simulation was conducted from 1300 (1400) LT for 42 (41) h from 12 to 18 March 2013. The initial 17 h of spin-up processes during the 2 km-NHM simulation were excluded from the analysis.

3. Results of observational campaign Period 3 (13 to 19 March 2013)

3.1 Validation of the model results

Figure 2 shows mean distributions of surface wind, sea surface pressure, and PWV during observational Period 3 derived from GANAL. No large-scale meteorological disturbances affected Java Island during the observational Period 3. PWV values around the Java Island were more than 50 mm. In this large-scale condition, distinct diurnal variations of precipitation and PWV were observed during the observational Period

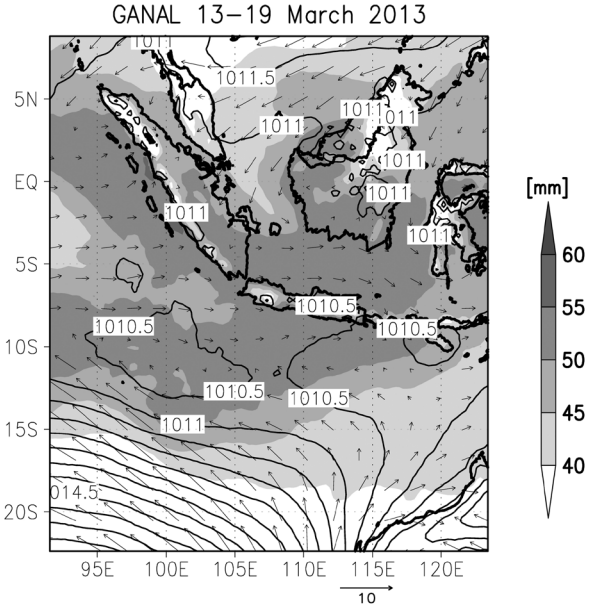

Fig. 2. Mean horizontal wind velocity at the surface (arrow), PWV (shade), and sea level pressure (contour line) derived from JMA global analysis during the observational Period 3.

3. Time variations of observed and simulated PWV at each of the seven stations during the observational Period 3 are presented in Fig. 3 shown in local time. A discontinuity occurs at 0700 LT every day due to the joining of the final 24 h of the 2 km-NHM simulations from consecutive days to present simulated PWV values. GNSS-derived PWV can be considered as a spatially averaged water vapor amount within an inverse cone centered by the GNSS receiver. Assuming the exponential decrease of the water vapor mixing ratio with height, approximately 63 % of PWV is contained in the height range below the e-folding

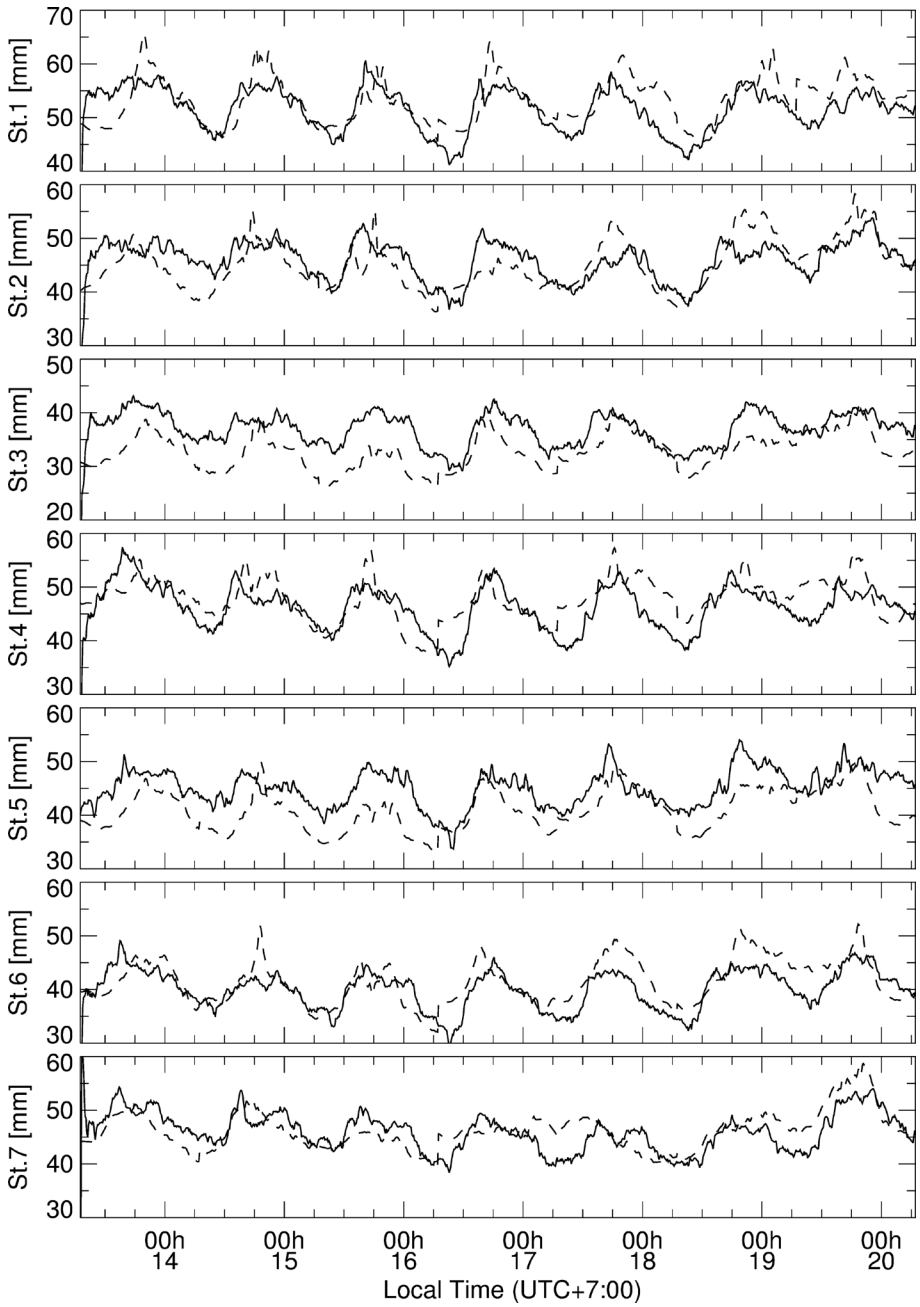

Fig. 3. Time variations of PWV observed by GNSS (solid line) and simulated by 2 km-NHM (broken line) at the seven stations.

scale height, which was estimated as 2.7 km from the 1 km horizontal resolution NHM data (Oigawa et al. 2014). The radius of the inverse cone at 2.7 km is 15 km in the case of 10° elevation angle cut-off, which can be defined in this study as the effective horizontal area of the GNSS-PWV measurements. In order to adjust the spatial resolution of the model PWV (2 km horizontal grid) to the GNSS-derived PWV, simulated PWV values were spatially averaged within a circle of 15 km radius centered at the GNSS stations. Then, the areal average of the model PWV values were compared with the GNSS-derived PWV values. Note that the simulated PWV values were corrected to account for height differences between the real ground and the model ground at the GNSS stations.

Diurnal PWV variations were observed at all stations where PWV values peaked during the evening, which were also simulated by the 2 km-NHM. Prior to 16 March, there were negative biases of PWV, particularly at stations 3 and 5 within the basin. However, simulation results improved after 16 March. The observed PWV variations were most closely simulated by 2 km-NHM on 16 March, with a mean difference of only −0.17 mm.

Figure 4 shows the time–height variations of the water vapor mixing ratio (Qv) around the basin observed by six hourly radiosondes (a) and that simulated by the 2 km-NHM (b). The radiosonde observation values were interpolated to the height of model layers to compare them with the simulation result. Horizontal extent of balloon trajectory could become as large as several tens of kilometers. Therefore, similar to the comparison in Fig. 3, the values of simulated Qv were averaged horizontally within a circle of 15-km radius centered at the balloon launch site. In the observation result, there existed a humid layer near the ground at 0700 LT. During the day, a convective mixed layer developed due to solar heating, which exceeded a height of 2 km ASL at 1300 LT. From 1300 to 1900 LT, the atmosphere within the basin between the height of 3 km to 8 km became very humid due to deep convection generated in the afternoon. In addition, water vapor amount near the ground increased from 1300 LT probably due to evaporation of rain water. Although the model well simulated the diurnal variation of water vapor near the ground, Qv values in the model between 3 and 5 km were relatively smaller before 16 March 2013. Figure 5 shows time variations of Qv derived from the radiosonde observation and the 2 km-NHM. The simulated Qv values above 3 km ASL on 14 and 15 March 2013 were smaller than the observation result. This caused a negative bias of

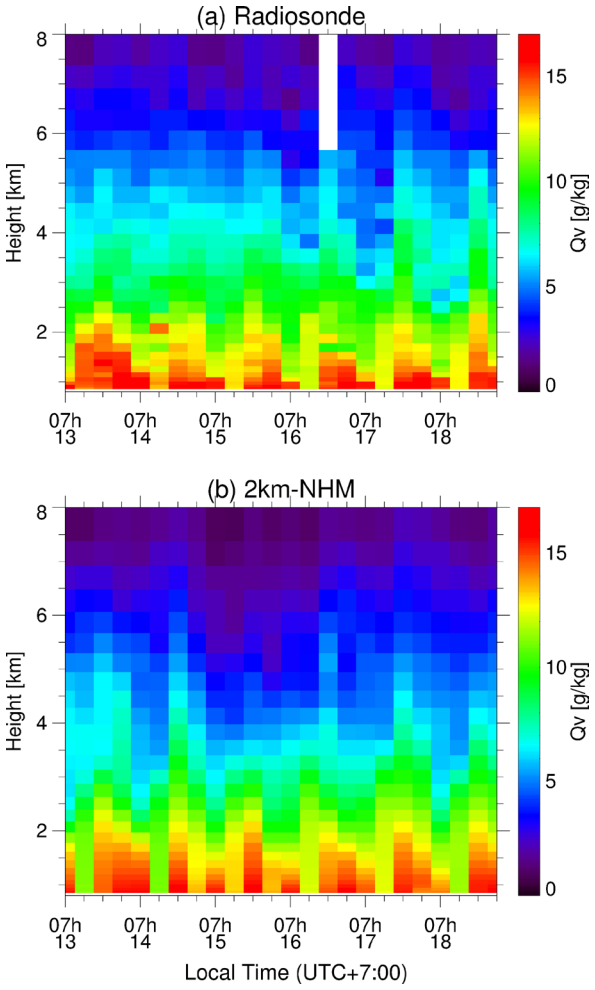

Fig. 4. (a) Time–height variation of Qv observed by six hourly radiosondes from 0700 LT on 13 to 0100 LT on 19 March 2013. The sonde observation values were interpolated to the height of model layers. (b) Time–height variation of Qv simulated by the 2-km-grid interval simulation every 6 h from 0700 LT on 13 to 0100 LT on 19 March 2013.

simulated PWV at the station 5 (Fig. 3). Nevertheless, the model data were worth using to analyze the diurnal variations of convective activity and water vapor, because the model well simulated the variation of water vapor below 3 km ASL that has large influences on convective activity.

Time variations of radar reflectivity and simulated rain rate in the Bandung region from 14 to 18 March 2013 were averaged throughout the area delimited by the rectangle within Fig. 1b (Figs. 6a, b). The radar

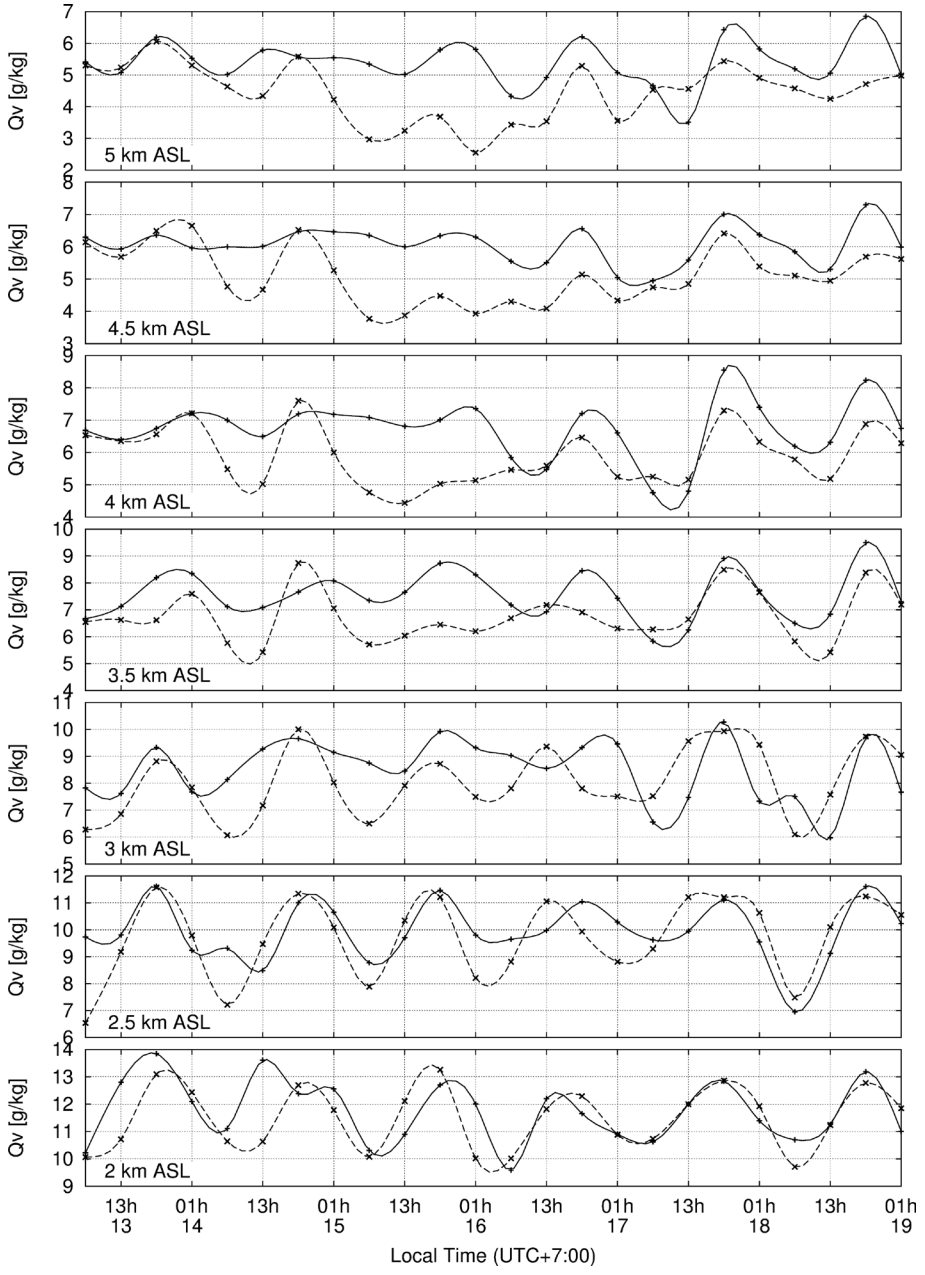

Fig. 5. Time variations of Qv observed by radiosonde (solid line) and simulated by 2 km-NHM (broken line) at heights of 2, 2.5, 3, 3.5, 4, 4.5, and 5 km ASL.

analysis indicated that rapid intensification of reflectivity occurred at approximately 1200 LT every day. Average reflectivity peaked in the evening and disappeared within the same day. The 2 km-NHM simulated the diurnal variation of rainfall that has a peak in the afternoon although relatively large time delays of onset of rainfall occurred on 14 and 18 March 2013. Time–latitude variations of radar reflectivity and simulated rain rate were averaged throughout the area delimited by the rectangle in Fig. 1b (Figs. 6c, d). Averaged topography within the rectangle is illustrated in Fig. 1c, indicating that the peaks of the northern and southern mountains are located at approximately 6.8°S and 7.16°S, respectively. The radar data suggest

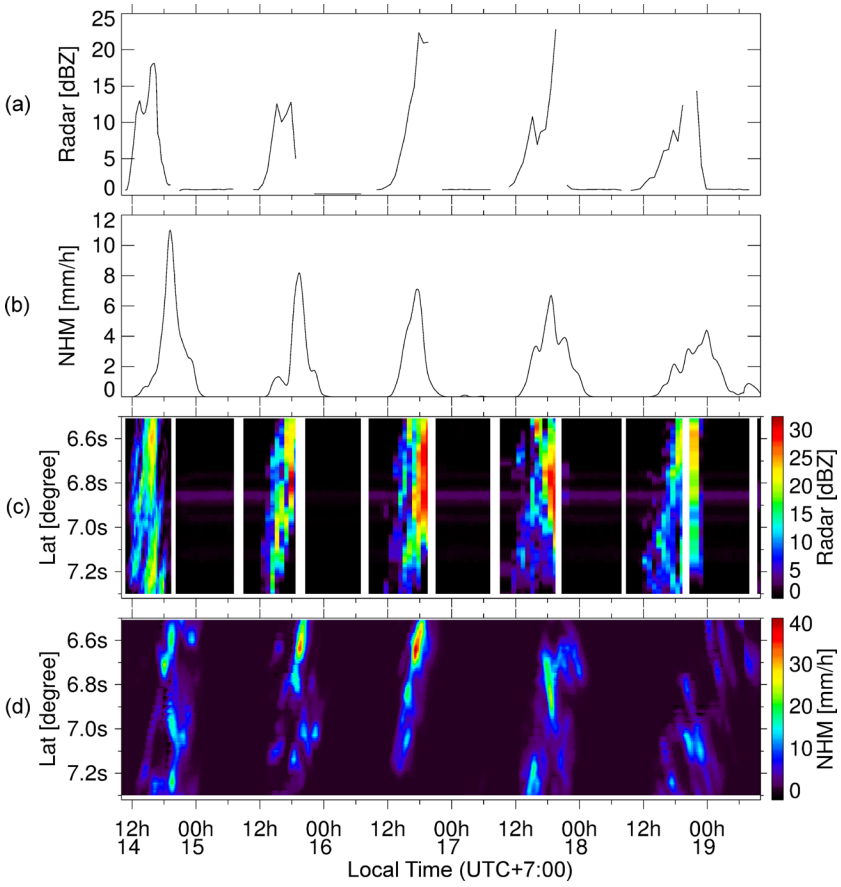

Fig. 6. Time variations of radar reflectivity (a) and simulated surface rain rate (b) averaged over the area delimited by the rectangle in Fig. 1b. Time–latitude variation of radar reflectivity (c) and simulated rain rate (d) averaged from 107.3–107.9°E within the area delimited by the rectangle in Fig. 1b. White spaces in (c) indicate periods when the radar was not operated.

that convection initiates at noon in the summit region of the southern mountains of Bandung. Most of the rain clouds were generated within this summit region from 15 to 17 March 2013. However, rain clouds can be observed that intruded into the basin from the southern mountains on 14 and 18 March 2013. The rainfall region within the southern mountains moved northward, merged with the convection generated around the northern mountains, and formed a widespread area of rainfall over the basin at approximately 1800 to 1900 LT. This broad rainfall area dissipated before 0000 LT. Convection initiation over the southern mountains and the northward movement of the rainfall area was well simulated by the 2 km-NHM for 15 to 17 March. However, for 14 and 18 March, there was a lag between simulated and observed rainfall activity (Fig. 6d). The simulation for 16 March accurately reproduced the timings of initiation, dissipation, and maximum level of the observed rainfall activity.

Maps of radar reflectivity observed every 100 min during 16 March are presented in Fig. 7. Convection initiation occurred at 1230 LT within the summit region of the southern mountains and in the east of the basin. At 1419 LT, isolated convective cells generated at the bottom of the basin and in the northern mountains. During the early evening (1604 LT), the isolated convective cells began to merge and a line-shaped rain cloud, extending west-southwest to east-northeast, was observed. Further, the high-reflectivity region gradually moved to the north of Bandung, and weak reflectivity spread over Bandung and the northern mountains (at 1750 and 1935 LT). The 2 km-NHM successfully reproduced convection initiation at 1230 LT over the southern mountains (Fig. 8). At 1410 LT,

isolated convective rainfall areas appeared within the bottom of the basin and in the northern mountains and began to merge at 1550 LT. As observed, the simulated rainfall area gradually moved to the north of Bandung, forming a widespread rainfall area over and north of Bandung during the evening. Using model data for 16 March, detailed analyses of water vapor variability and deep convection were undertaken to investigate the mechanisms of convective activity related to diurnal variation in Bandung.

3.2 Analysis of water vapor variability and low-level wind

Figure 9 shows the horizontal distribution of Qv and the horizontal wind velocity near the ground level, while Fig. 10 is the latitude–height section of the Qv and the vertical-northward wind velocity vector on 16 March from 2 km-NHM. The cross-section in Fig. 10 is obtained along the line A–B in the Fig. 8 where the first convection began ("CI") at the southern mountain at 1230 LT in the 2 km-NHM. In the morning at 0800 LT, humid air greater than 15 g kg^{-1} existed close to the ground level of the basin. Northward winds blew within the free atmosphere throughout the day (Fig. 10). At 1000 LT, an upslope wind was generated within the basin (Fig. 9). This upslope wind was formed by valley wind circulations in Fig. 10 that were especially strong on the northern slopes of the mountains. At 1200 LT, immediately before the convection initiation, the valley wind circulation was well developed, and low-level wind convergence occurred near the summits (lines A and B in Fig. 9). The convective mixed layer was locally deepened just above the low-level convergence zone. Humid air at the bottom of the basin seen during the morning was advected to the northern slope of the southern mountains by the valley wind. However, humidity close to ground level around the northern part of the basin decreased after 1000 LT due to downward valley wind circulation. A similar variation in humidity was also observed on the slopes near the plain area. Sea breeze from the Java Sea had not yet reached Bandung at 1200 LT. At 1400 LT, the upslope winds decreased in velocity on the southern slopes of the basin. Divergent flow was observed within the bottom of the basin (Fig. 9). Figure 10 suggests that the divergent flow within the basin at 1400 LT was caused by downdrafts associated with rainfall. The upslope wind in the northern mountains disappeared at 1600 LT (Fig. 9), when precipitation intensity became strong around the northern mountain of Bandung (Fig. 8). Downdraft from the rain clouds occurred over the northern mountains at 1600 LT, which converged with the breeze from the Java Sea shown by the line C in Fig. 9. At 1800 LT, low-level convergence between the cold air outflow from the rain clouds (figure not shown) and the sea breeze indicated by the line D in Fig. 9 was observed, which is a plausible triggering mechanism of evening convection over the plain (Wu et al. 2007). Rainfall over the plain continued until late evening.

These results suggest that valley wind circulation over the southern basin possibly affected convection initiation on 16 March, by advecting moisture and causing the formation of a deep mixed layer. Further analyses were necessary to investigate whether the simulated moisture variation also occurred on days other than 16 March during observational Period 3. Time–latitude variation of the rate of increasing PWV values, and low-level wind divergence from 2 km-NHM are presented in Fig. 11. On 16 March, PWV over the southern mountains increased prior to 1200 LT. From 1230 to 1800 LT, a region of PWV with a high increase rate moved northward due to propagation of the rainfall area. PWV decreased after 1800 LT, suggesting that the convection weakened. In the wind field, low-level convergence, induced by valley wind, occurred over the northern slopes of the mountains. Convergence over the southern mountains is stronger than over the northern mountains. After 1230 LT, the convergent region also propagated northward. Low-level convergence and PWV increase at the summit of the southern mountains were both analyzed on 15 and 17 March 2013.

Time–height variation of the Qv in 2 km-NHM within the northern, bottom and southern parts of the basin are presented in Fig. 12. Low-level moisture was shown to decrease within the bottom and northern parts of the basin and was shown to increase in the southern part of the basin from 0700 to 1200 LT on 16 March due to valley wind circulation. This water vapor variation within the basin prior to convection initiation can be also seen for 15 and 17 March.

4. Discussion

4.1 Effect of moisture on the convective activity inside the basin

Trilaksono et al. (2012) conducted ensemble simulations using a regional nonhydrostatic model to reproduce heavy rainfall over West Java in January–February 2007 in which the initial 18 h data were excluded from the analysis to avoid the effects of unrealistic convection during the spin-up process. Our study also set the spin-up time as 17 h and succeeded in reproducing the diurnal variation of convective ac-

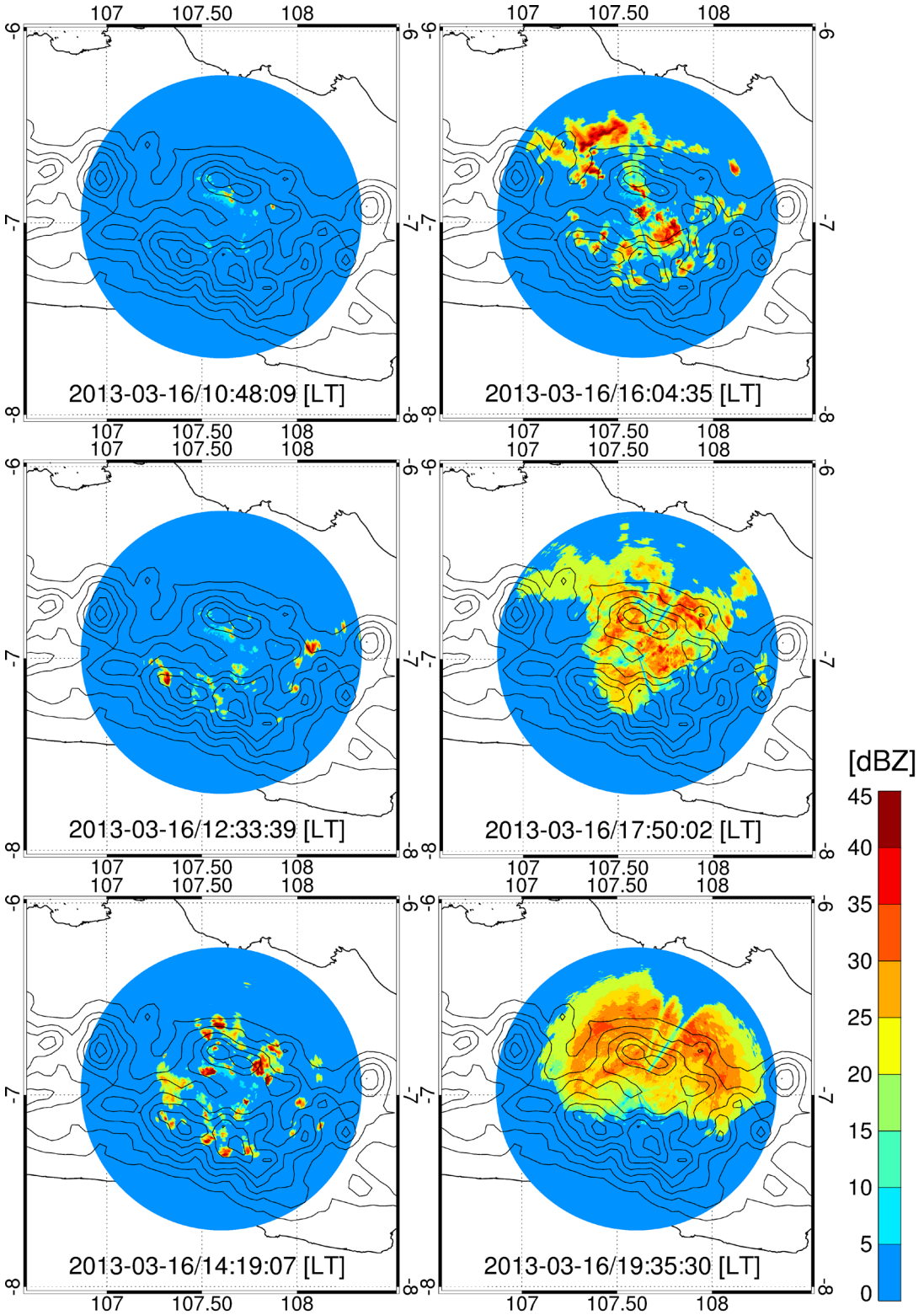

Fig. 7. Maps of radar reflectivity from 1048 LT to 1935 LT every 100 min on 16 March 2013. The elevation angle of the PPI scan was 5°. Contours show the elevation of the topography every 250 m.

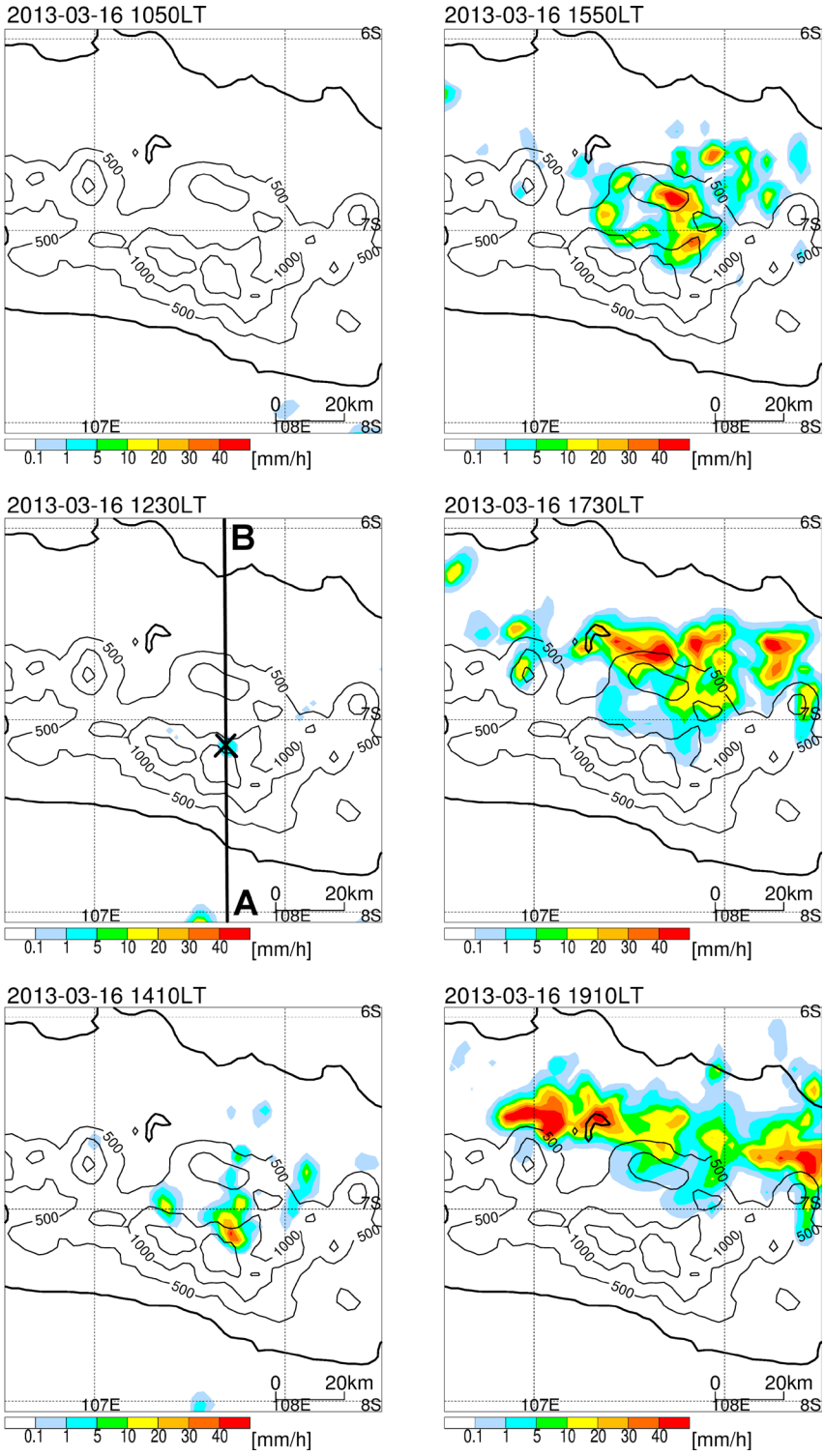

Fig. 8. Maps of the rain rate simulated by 2 km-NHM from 1050 LT (the top left) to 1910 LT (the bottom right) every 100 min on 16 March 2013. The line A–B corresponds to the vertical cross-section of Fig. 10. The symbol "X" indicates the location of the first convection, referred as "CI" in the text. Contours show the elevation of the topography every 500 m.

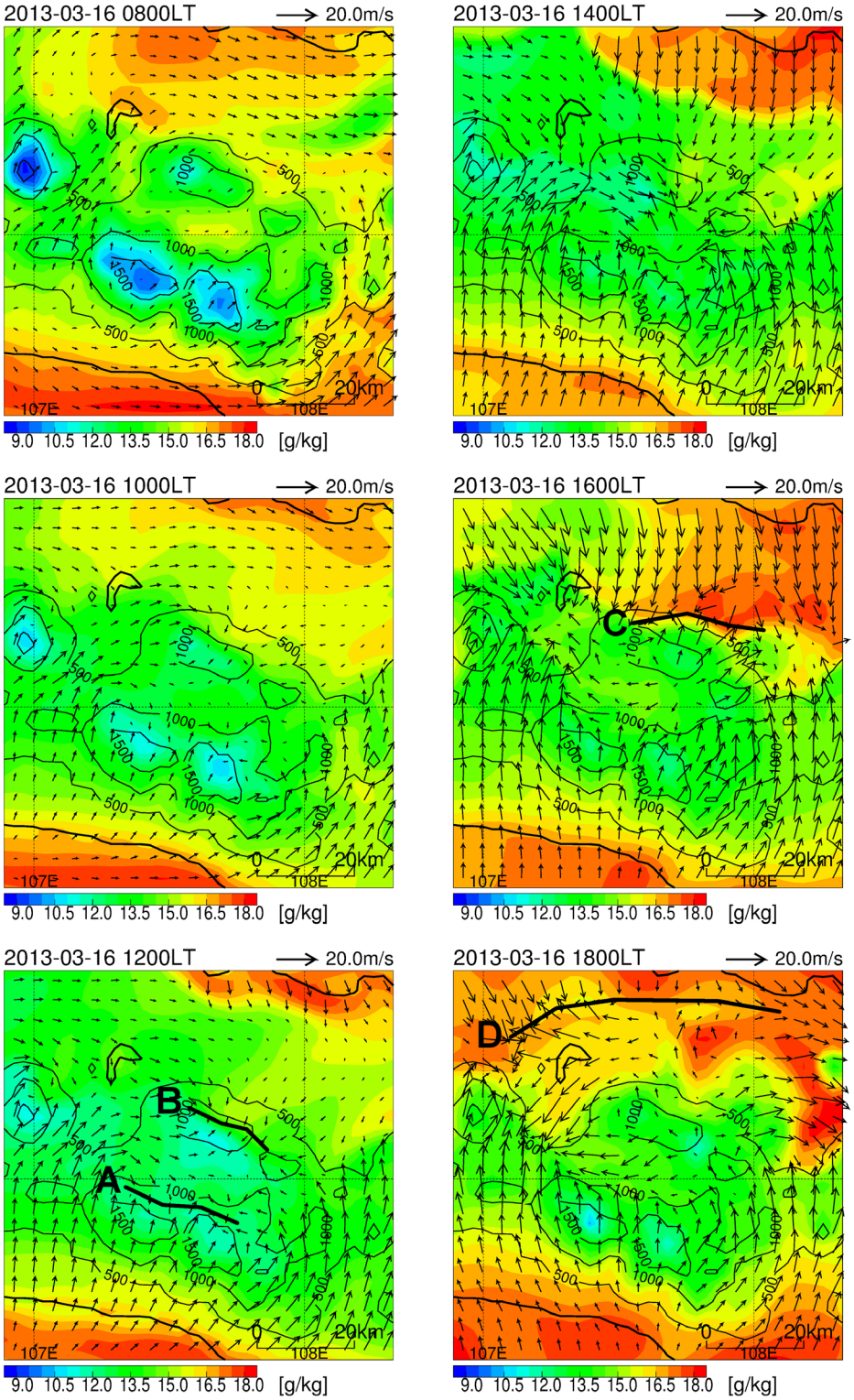

Fig. 9. Maps of Qv (color contour) and horizontal wind velocity (arrow) at a height of 288 m simulated by 2 km-NHM every 100 min from 1050 LT (the top left) to 1910 LT (the bottom right) on 16 March 2013. Contours represent ground levels every 500 m. Black lines A, B, C, and D represent convergence lines of horizontal winds.

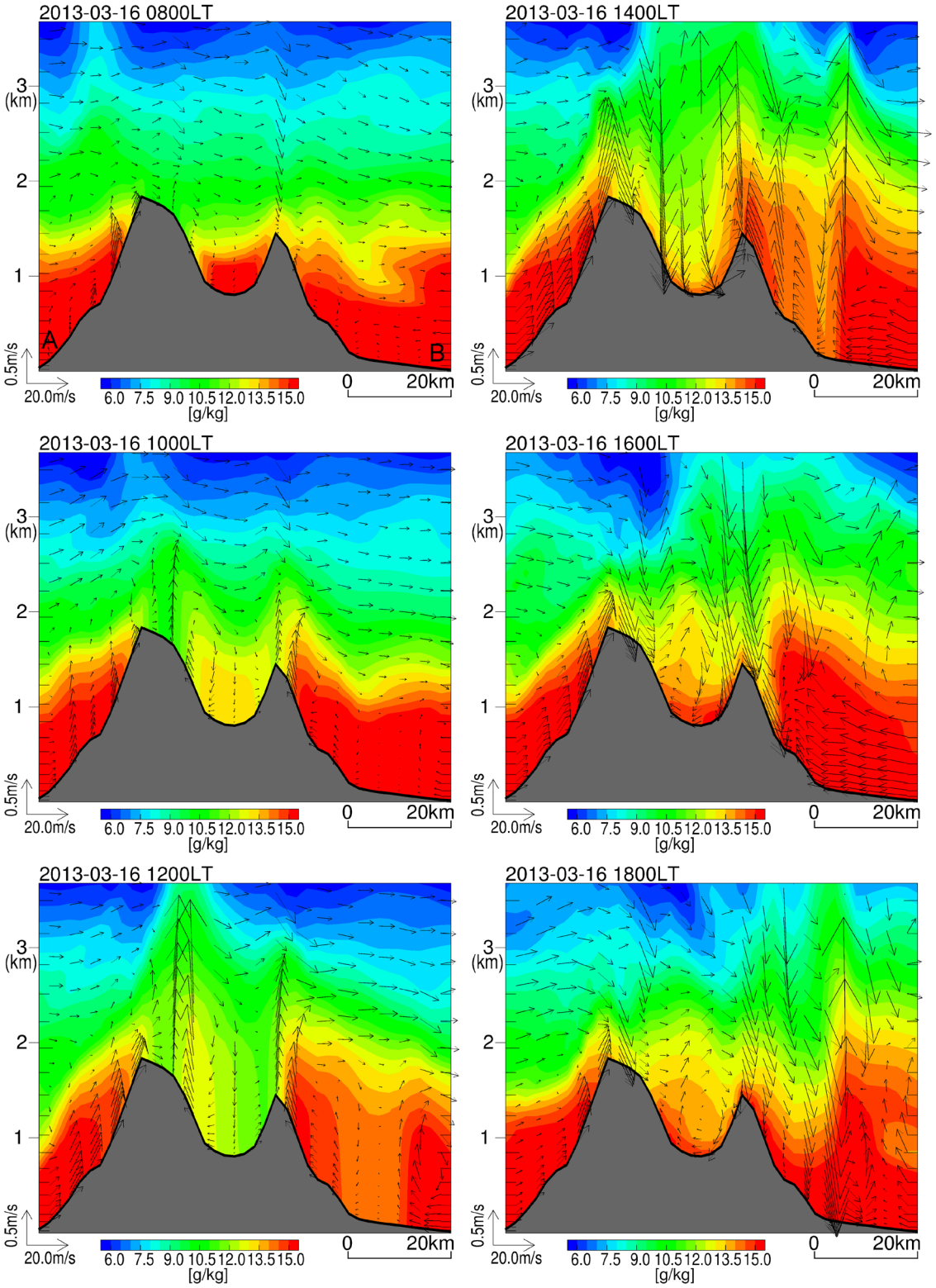

Fig. 10. Latitude–height section along line A–B in Fig. 8. The Qv (color contour) and wind velocity (arrow) every 2 h from 0800 LT (the top left) to 1800 LT (the bottom right) on 16 March 2013.

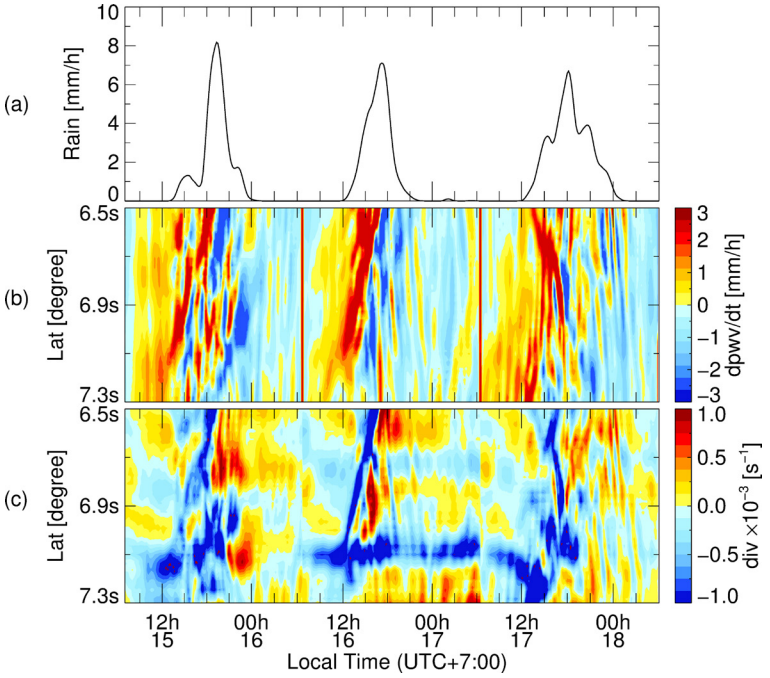

Fig. 11. (a) Time variation of simulated surface rain rate averaged across the area delimited by the rectangle in Fig. 1b. Time–latitude variation of (b) increase rate of PWV, and (c) horizontal wind divergence at 288 m AGL simulated by 2 km-NHM averaged from 107.3–107.9°E within the area delimited by the rectangle in Fig. 1b.

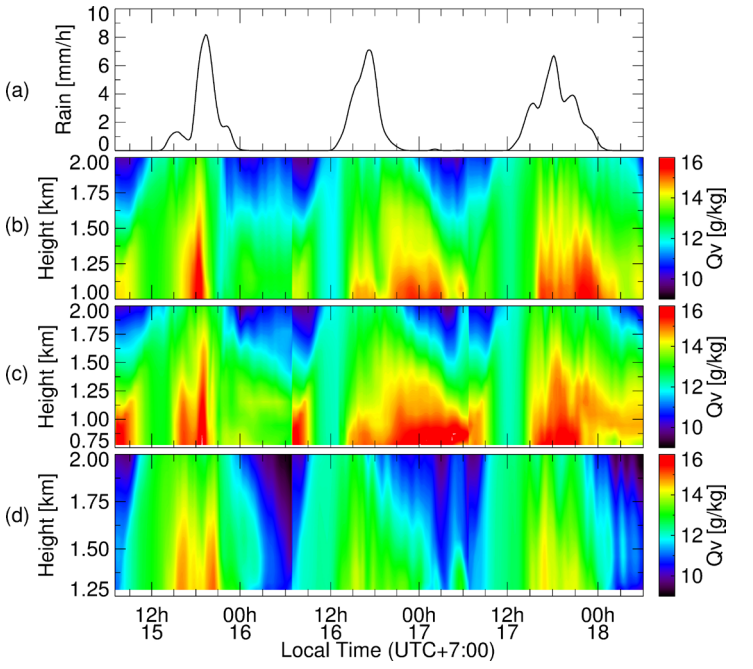

Fig. 12. (a) Time variation of simulated surface rain rate averaged over the area delimited by the rectangle in Fig. 1b. Time–height variation of Qv simulated by 2 km-NHM at (b) the northern basin, (c) the bottom of the basin, and (d) the southern basin averaged along the lines A, B, and C, respectively, in Fig. 1b.

tivity. We also tested another downscaling simulation starting at 0800 LT on 16 March 2013 with no spin-up time (hereafter, "2 km-NHM-nosp") to examine the necessary spin-up interval of the model (see Appendix for details). In this case, the initiation of convection occurred at 1530 LT, which was delayed by 3 h compared to the observed event (see Fig. A1). We found that the spin-up interval of approximately 18 h was necessary to simulate well the diurnal cycle of convection.

Figure 13 shows vertical profiles of potential temperature, equivalent potential temperature, and saturated equivalent potential temperature at "CI" at 0800 LT and 1200 LT on 16 March 2013 simulated by 2 km-NHM. Air parcels near the ground had no level of free convection (LFC) at 0800 LT (Fig. 13a). At 1200 LT, equivalent potential temperature below the height of 4 km increased and the atmospheric profile became unstable (Fig. 13b). In the 2 km-NHM simulation at "CI", the convective available potential energy (CAPE) of an air parcel at 2 km ASL was 272 J kg^{-1} and the distance from the parcel's altitude to its LFC was 173 m at 1200 LT on 16 March. In contrast, the static stability of 2 km-NHM-nosp at 1200 LT at "CI" was higher than that of 2 km-NHM because increase amount of equivalent potential temperature near the ground was small, compared to that simulated by 2 km-NHM (see Fig. A2). The CAPE was approximately four times less (63 J kg^{-1}), and the LFC was approximately two times greater (375 m).

The 2 km-NHM simulation that started at 1400 LT on 15 March 2013 with a 17 h spin-up accurately reproduced a radiosonde-measured Qv value close to the ground within the basin at 0700 LT on 16 March, whereas that of 2 km-NHM-nosp was approximately 3 g kg^{-1} smaller than the observation result (see Fig. A3). In 2 km-NHM, the moisture near the ground within the basin was advected to the southern slope of the basin by the valley wind circulation as already shown in Figs. 10 and 12, resulting in increase of Qv at "CI" and decrease of Qv at the bottom basin at 1200 LT in 2 km-NHM. In contrast, in the 2 km-NHM-nosp, increase of Qv near the ground at "CI" and associated destabilization of the atmosphere were too small to initiate convection at 1230 LT on 16 March 2013 despite the occurrence of the low-level wind convergence due to the valley wind (not shown). These results suggest that the spin-up interval should be long enough to reproduce the atmospheric conditions inside the basin from the previous day. Moisture amount at the bottom of the basin in the morning is important because the static stability was reduced by the advection of moisture to the southern part of the basin by the valley wind.

Earlier studies reported that many general circulation models (GCMs) tended to show a peak of diurnal precipitation cycle during mid-day, although observations indicated the rain peak late in the afternoon (Dai 2006). Covey et al. (2016) also found the problem of the too-early rainfall even in the recent high-resolution

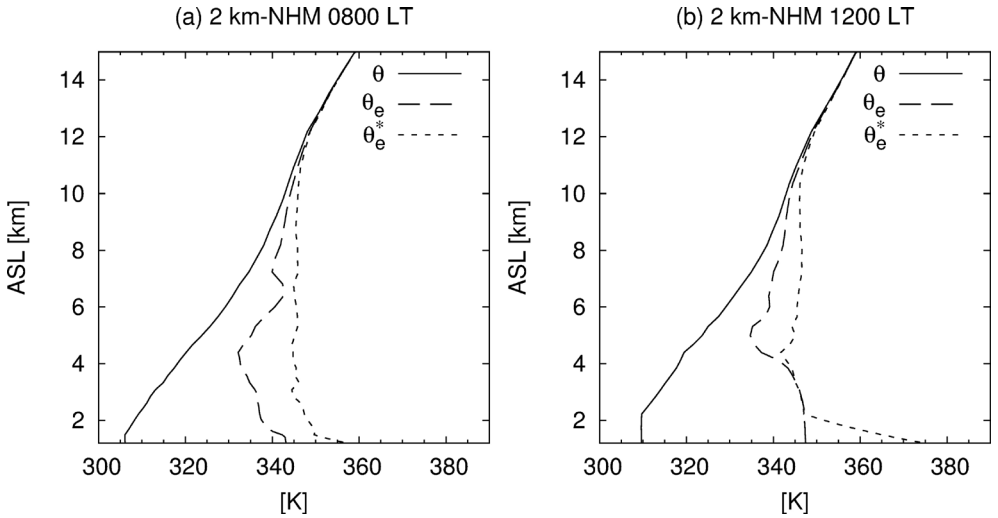

Fig. 13. Vertical profiles of potential temperature (θ), equivalent potential temperature (θe), and saturated equivalent potential temperature (θe*) at "CI" at 0800 LT on 16 March 2013 (a) and 1200 LT on 16 March 2013 (b) simulated by 2 km-NHM.

GCMs with a 20-km mesh, suggesting that sub-grid scale parameterizations are responsible for the model error. In this study, the initiation timing of afternoon convection around Bandung was successfully simulated, because low-level wind convergence induced by the valley wind circulation was well reproduced by 2 km-NHM. In contrast, the outer model (15 km-NHM) failed to reproduce the afternoon convection probably because the valley wind circulation inside the basin was not established well due to poor reproduction of the topography of the Bandung basin. By reducing the mesh size down to 3.5 km, Sato et al. (2009) reproduced the initiation timing of afternoon convection over land using NICAM and suggested that it is important to explicitly resolve the shallow cumulus at the top of the convective mixed layer and associated vertical transport of moisture by the cumulus cloud. These investigations suggest that the peak time of rainfall over land can be reproduced by making the horizontal mesh size as short as 2 km, which is enough to explicitly resolve the cumulus clouds instead of using a cumulus parameterization scheme.

4.2 Mechanism of diurnal variation of PWV over the complex terrain

The averaged diurnal variations of PWV at stations 3, 4, 5, and 6 during the period from March 15 to 17 are presented in Fig. 14. Distinct diurnal variations of PWV exhibited a single peak during 1800–1900 LT. This result is consistent with previous studies that investigated the diurnal variation of PWV near mountain regions (Iwasaki 2001; Wu et al. 2003). During 0900–1200 LT, PWV at station 6, located in the southern part of the basin, increased by approximately 3 mm, whereas PWV at station 3, located in the northern basin near the mountain slope, almost remained unchanged. After 1200 LT, PWV abruptly increased at stations 4 and 6, located on the northern side of mountains where slopes were heated by solar radiation during this season. Abrupt increases of PWV at stations 3 and 5, located on the southern side of mountains, also occurred; however, the onset timings were delayed by 1–2 h. From the GNSS observations, the time variations of PWV are not spatially uniform, even inside a small basin like Bandung.

Figure 15 shows a map of the increase in PWV during 0900–1200 LT on March 16 in the 2 km-NHM simulation. As with the GNSS observations, PWV increased particularly in the southern part of the basin and decreased in the northern part of the basin, suggesting that the model simulation successfully reproduced the diurnal variations of PWV and its

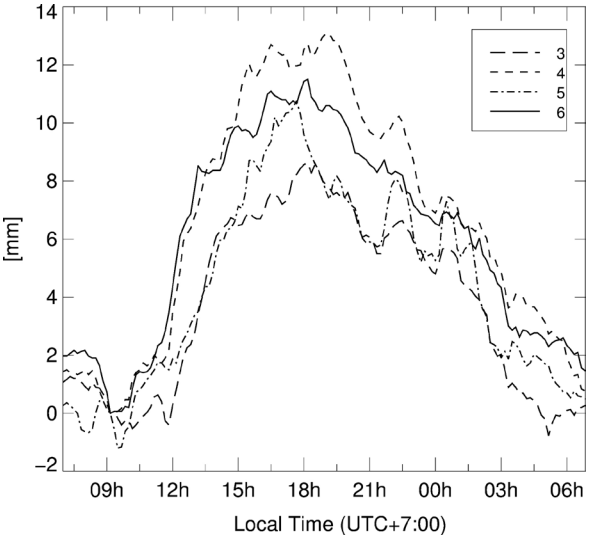

Fig. 14. Diurnal variations of GNSS-derived PWV averaged during 15 to 17 March 2013 at the GNSS stations 3, 4, 5, and 6 in Fig. 1b. Note that the increment of PWV relative to the value at 0900 LT at each station is shown.

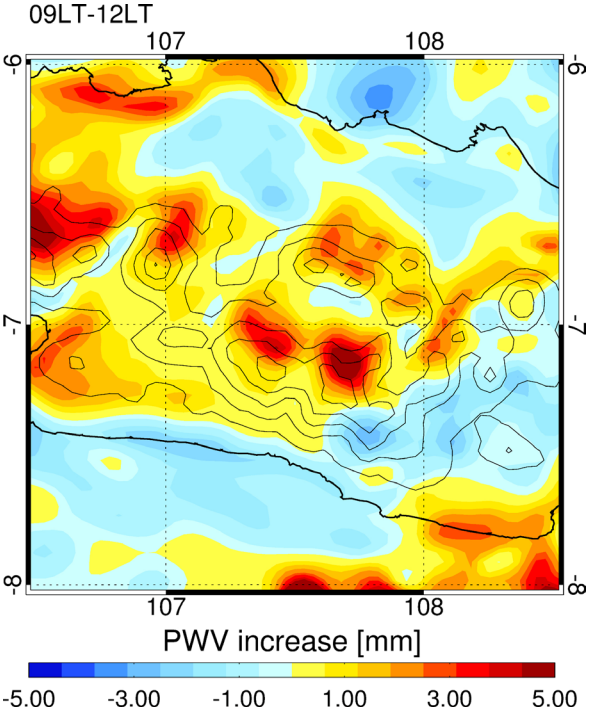

Fig. 15. PWV increase from 0900 LT to 1200 LT on 16 March 2013 in 2 km-NHM.

geographical pattern around Bandung. The increase in PWV in the southern part of the basin was caused by low-level moisture convergence induced by the valley wind circulation, which is the same mechanism reported by previous studies (Iwasaki and Miki 2001; Wu et al. 2003; Iwasaki 2004; Sato and Kimura 2005). Conversely, PWV in the northern basin decreased, although GNSS station 3 was under the influence of the valley wind circulation of the northern basin. As shown in Fig. 10, the spatial scale of the valley wind circulation in the southern basin is larger than that in the northern part of the basin. Therefore, it is suggested that most of the water vapor that existed at the bottom of the basin in the morning was advected to the southern part of the basin by the larger valley wind circulation, and PWV in the northern part of the basin decreased due to the downward movement of dry air by the circulation. The valley wind circulation in the southern basin was larger probably because the top of the southern mountain is higher than the northern mountain. Another possible explanation is that the southern slope of Bandung was more efficiently heated by the solar radiation, as the azimuth and elevation angles of the sun around Bandung at 1200 LT on 16 March 2013 were approximately 354° and 85°, respectively. Idealized numerical simulation experiment is needed to investigate the effects of solar position and mountain height differences.

Iwasaki (2004) reported that the diurnal variation of PWV around Mt. Tanigawa has dual peaks. The first peak is caused by the valley wind, and the second peak is caused by the "extended sea breeze." In contrast, the diurnal variation of PWV around Bandung has a single peak probably because the mountains surrounding the basin inhibited the effect of moisture convergence due to the sea breeze on the increase in PWV.

5. Summary

Mechanisms of diurnal variation in water vapor and tropical deep convection over a complex terrain were investigated by analyzing detailed observations and high-resolution numerical model data. An observational campaign was conducted during the rainy season of 2013. A numerical downscaling experiment was also conducted using JMA-NHM to reproduce the diurnal cycle of rainfall observed during the observational Period 3, from 13 to 19 March 2013. During this period, distinct diurnal variation was observed without the influence of large-scale disturbances, such as MJO. To correctly represent the complex topography of the Bandung basin, a downscaling simulation with a 2-km-horizontal mesh was adopted.

The simulation results underestimated PWV values within the basin during the first half of Period 3. However, diurnal cycles of PWV were successfully reproduced because moisture amount below 3 km ASL was well simulated by the model. For 16 March, 2 km-NHM closely simulated the observed PWV variations with a mean difference of only −0.17 mm. The X-band radar observed a diurnal cycle of precipitation over the basin, which reached its peak at approximately 1800 LT. Convection initiated at noon over the summit of the southern mountain of Bandung and caused widespread rainfall across the northern part of the basin during the evening. The model succeeded in simulating the observed rainfall activity for 15 to 17 March 2013. Detailed analysis of water vapor variability and deep convection on 16 March were performed to investigate the mechanism of diurnal convective activity in Bandung. The model data successfully reproduced deep convection from initiation to dissipation.

Model results for 16 March 2013 indicated that static stability over the southern slope of the basin decreased due to moisture transport from the bottom part of the basin by a thermally-induced circulation. The circulation formed low-level wind convergence with a deepened, moist convective mixed layer within the southern parts of the basin and decreased humidity within the northern part of the basin. In addition, water vapor variations within the basin, caused by valley winds, were also analyzed on 15 and 17 March 2013. The GNSS receiver network also observed the simulated water vapor variability. These results suggest that water vapor within the bottom of the basin during the morning, and low-level wind convergence induced by valley winds are important factors of convection initiation in Bandung.

Acknowledgments

The numerical model used in this study was provided by JMA. The Meteorological Research Consortium provided the initial and boundary condition data. The Meteorological Research Institute developed the drawing tool for the JMA-NHM (mplot). Radiosonde data were plotted by using analysis software developed by the Inter-university Upper Atmosphere Global Observation Network (IUGONET). The authors express their sincere gratitude to Dr. Atsuki Shimbori of Kyoto University for his support in using the IUGONET analysis software. We would like to offer our special thanks to Dr. Tri Wahyu Hadi of Institute Technology Bandung, Indonesia, for his valuable

comments. Thanks are also extended to Professor Hirohiko Ishikawa, Disaster Prevention Research Institute, Kyoto University, for providing valuable insight on the numerical simulation results, and Dr. Yoshinori Shoji, Dr. Hiromu Seko, Dr. Takuya Kawabata and Dr. Masaru Kunii (MRI) for useful discussions. This work is partially supported by JSPS KAKENHI Grant Numbers JP15H03724.

Appendix

In addition to the numerical experiment described in the text, we also conducted another downscaling simulation to reproduce precipitation on 16 March 2013. The 15-km-mesh outer model initialized at 0700 LT on 16 March 2013 and 2-km-mesh inner model initialized at 0800 LT on 16 March 2013. The result of 2-km-mesh model data from the initial time was used for analysis without considering the spin-up. This 2-km-mesh simulation is hereinafter called as "2 km-NHM-nosp." The start time of rainfall in 2 km-NHM-nosp delayed by approximately 3 h compared to that simulated by 2 km-NHM (Fig. A1). Compared to 2 km-NHM, static stability of the atmosphere at the mountain slope "CI" at 1200 LT was higher in 2 km-NHM-nosp, because the equivalent potential temperature near the ground was small (Fig. A2). The air parcel at the 2 km ASL at "CI" has an LFC of 375 m and CAPE of 63 g kg^{-1}.

Fig. A3 shows the vertical profiles of temperature and water vapor mixing ratio (Qv) at 0800 LT and 1200 LT on 16 March 2013 simulated by 2 km-NHM and 2 km-NHM-nosp. Large difference can be seen in the moisture amount at 0800 LT at the bottom basin (station 5) between the two experiments although temperature profiles were nearly the same. Moist air

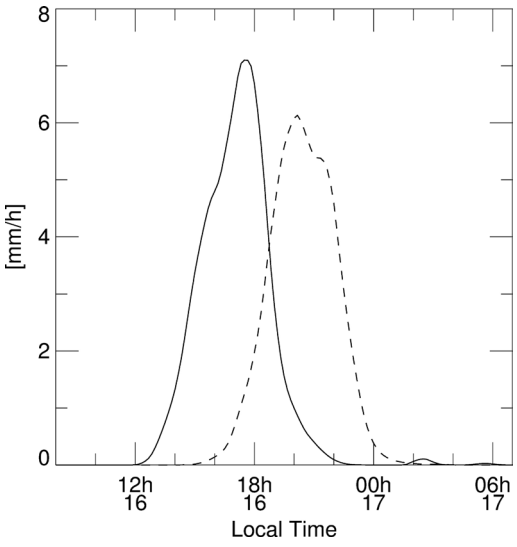

Fig. A1. Time variations of the simulated surface rain rate averaged over the area delimited by the rectangle in Fig. 1b. Solid and broken lines correspond with the result of 2 km-NHM and 2 km-NHM-nosp.

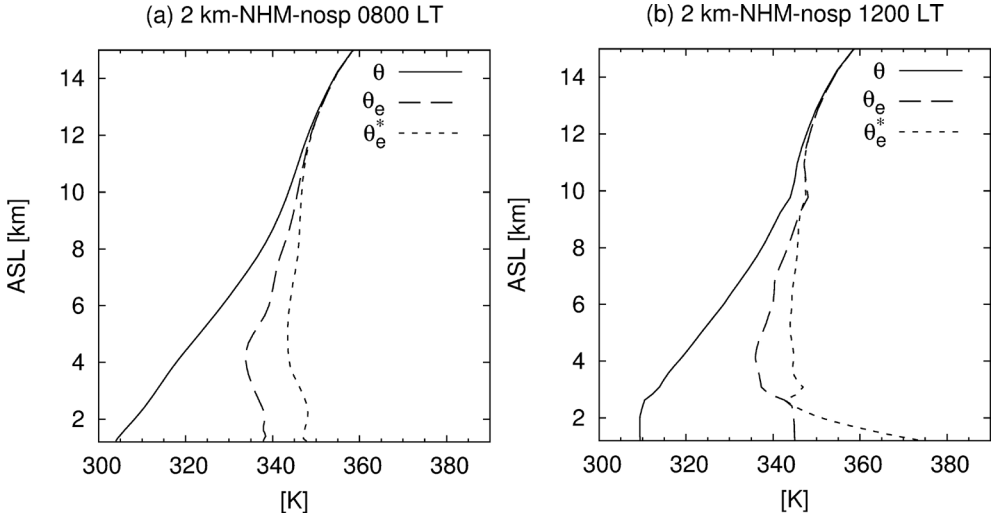

Fig. A2. Vertical profiles of potential temperature (θ), equivalent potential temperature (θe), and saturated equivalent potential temperature (θe*) at "CI" at 0800 LT and 1200 LT on 16 March 2013 simulated by 2 km-NHM-nosp.

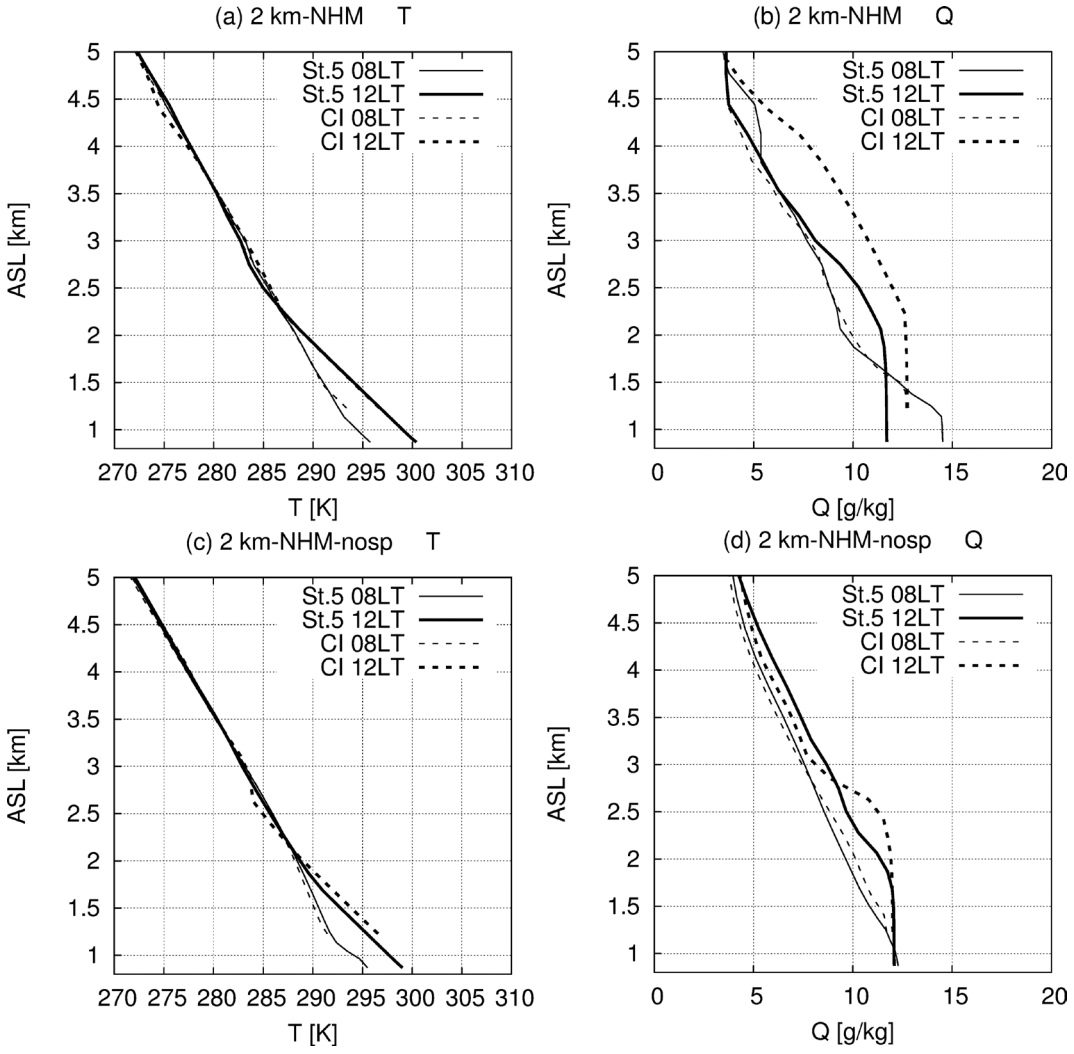

Fig. A3. Vertical profiles of temperature (a and c) and water vapor mixing ratio (b and d) at 0800 LT and 1200 LT on 16 March 2016 simulated by 2 km-NHM and 2 km-NHM-nosp. Profiles at "CI" and station 5 are shown.

existed near the ground at station 5 at 0800 LT in 2 km-NHM. However, in 2 km-NHM-nosp, Qv values below 2 km ASL were smaller than that of 2 km-NHM (Figs. A3b, d). In 2 km-NHM at 1200 LT, the moisture amount at "CI" was larger than that at station 5 because of the moisture transport by the valley wind circulation. In contrast, in 2 km-NHM-nosp, the moisture amount at "CI" at 1200 LT is as same as that at station 5 because of the smaller moisture amount at the bottom of the basin in the morning. This small moisture amount at "CI" at 1200 LT caused the small equivalent potential temperature near the ground and large static stability, resulting in a 3 h delay of convection initiation in 2 km-NHM-nosp. These results suggest that the timing of convection initiation in Bandung in the model is sensitive to the moisture amount at the bottom of the basin in the morning. Therefore, the spin-up interval of the model is important to reproduce the moisture amount at the bottom of the basin that is affected by the convective activity in the previous day.

References

Bevis, M., S. Businger, T. A. Herring, C. Rocken, R. A. Anthes, and R. H. Ware, 1992: GPS Meteorology: Remote sensing of atmospheric water vapor using the global positioning system. *J. Geophys. Res.*, **97**, 15787–15801.

Covey, C., P. J. Gleckler, C. Doutriaux, D. N. Williams, A. Dai, J. Fasullo, K. Trenberth, and A. Berg, 2016: Metrics for the diurnal cycle of precipitation: Toward routine benchmarks for climate models. *J. Climate*, **29**, 4461–4471.

Dai, A., 2006: Precipitation characteristics in eighteen coupled climate models. *J. Climate*, **19**, 4605–4630.

Dai, A., F. Giorgi, and K. E. Trenberth, 1999: Observed and model simulated precipitation diurnal cycle over the contiguous United States. *J. Geophys. Res.*, **104**, 6377–6402.

Dai, A., J. Wang, R. H. Ware, and T. Van Hove, 2002: Diurnal variation in water vapor over North America and its implications for sampling errors in radiosonde humidity. *J. Geophys. Res.*, **107**, 4090, doi:10.1029/2001JD000642.

Fujibe, F., 1988: Diurnal variations of precipitation and thunderstorm frequency in Japan in the warm season. *Pap. Meteor. Geophys.*, **39**, 79–94.

Fujita, M., K. Yoneyama, S. Mori, T. Nasuno, and M. Satoh, 2011: Diurnal convection peaks over the eastern Indian Ocean off Sumatra during different MJO phases. *J. Meteor. Soc. Japan*, **89**, 317–330.

Holland, G. J., and T. D. Keenan, 1980: Diurnal variations of convection over the "Maritime Continent". *Mon. Wea. Rev.*, **108**, 223–225.

Houze, Jr., R. A., S. G. Geotis, F. D. Marks, Jr., and A. K. West, 1981: Winter monsoon convection in the vicinity of North Borneo. Part I: Structure and time variation of the clouds and precipitation. *Mon. Wea. Rev.*, **109**, 1595–1614.

Iwasaki, H., 2004: Diurnal variation of precipitable water and convective activity with dual maxima in summer season around Mt. Tanigawa in the northern Kanto District, Japan. *J. Meteor. Soc. Japan*, **82**, 805–816.

Iwasaki, H., and T. Miki, 2001: Observational study on the diurnal variation in precipitable water associated with the thermally-induced local circulation. *J. Meteor. Soc. Japan*, **79**, 1077–1091.

Japan Meteorological Agency, 2013: Outline of the operational numerical weather prediction at the Japan Meteorological Agency. *WMO Technical Progress Report on the Global Data Processing and Forecasting System (GDPFS) and Numerical Weather Prediction (NWP) Research*, 28–36.

Kain, J. S., and J. M. Fritsch, 1993: Convective parameterization for mesoscale models: The Kain-Fritsch scheme. *The representation of cumulus convection in numerical models*. Meteor. Monogr., **24**, Amer. Meteor. Soc., 165–170.

Kondo, H., 1990: A numerical experiment of the "extended sea breeze" over the Kanto Plain. *J. Meteor. Soc. Japan*, **68**, 419–434.

Lin, Y.-L., R. D. Farley, and H. D. Orville, 1983: Bulk parameterization of the snow fields in a cloud model. *J. Climate. Appl. Meteor.*, **22**, 1065–1092.

Murakami, M., 1990: Numerical modeling of dynamical and microphysical evolution of an isolated convective cloud–the 19 July 1981 CCOPE cloud. *J. Meteor. Soc. Japan*, **68**, 107–128.

Nakanishi, M., and H. Niino, 2006: An improved Mellor-Yamada Level-3 model: Its numerical stability and application to a regional prediction of advection fog. *Bound.-Layer Meteor.*, **119**, 397–407.

Oigawa, M., E. Realini, H. Seko, and T. Tsuda, 2014: Numerical simulation on retrieval of meso-γ scale precipitable water vapor distribution with the Quasi-Zenith Satellite System (QZSS). *J. Meteor. Soc. Japan*, **92**, 189–205.

Realini, E., K. Sato, T. Tsuda, Susilo, and T. Manik, 2014: An observation campaign of precipitable water vapor with multiple GPS receivers in western Java, Indonesia. *Prog. Earth. Planet. Sci.*, **1**, 17, doi:10.1186/2197-4284-1-17.

Rocken, C., L. Mervart, Z. Lukes, J. Johnson, M. Kanzaki, H. Kakimoto, and Y. Iotake, 2001: Testing a new network RTK software system. *Proceedings of the 17th International Technical Meeting of the Satellite Division of The Institute of Navigation (ION GNSS 2004)*, Long Beach, CA, 2831–2839.

Saito, K., T. Keenan, G. Holland, and K. Puri, 2001: Numerical simulation of the diurnal evolution of tropical island convection over the Maritime Continent. *Mon. Wea. Rev.*, **129**, 378–400.

Saito, K., T. Fujita, Y. Yamada, J. Ishida, Y. Kumagai, K. Aranami, S. Ohmori, R. Nagasawa, S. Kumagai, C. Muroi, T. Kato, H. Eito, and Y. Yamazaki, 2006: The operational JMA nonhydrostatic mesoscale model. *Mon. Wea. Rev.*, **134**, 1266–1298.

Saitoh, T., and F. Kimura, 1998: Diurnal variation of convective precipitation in Chubu-Kanto area in the summer. *Tenki*, **45**, 541–549 (in Japanese).

Sato, T., and F. Kimura, 2003: A two-dimensional numerical study on diurnal cycle of mountain lee precipitation. *J. Atmos. Sci.*, **60**, 1992–2003.

Sato, T., and F. Kimura, 2005: Diurnal cycle of convective instability around the central mountains in Japan during the warm season. *J. Atmos. Sci.*, **62**, 1626–1636.

Sato, T., H. Miura, M. Satoh, Y. N. Takayabu, and Y. Wang, 2009: Diurnal cycle of precipitation in the tropics simulated in a global cloud-resolving model. *J. Climate*, **22**, 4809–4826.

Takayabu, Y. N., 2002: Spectral representation of rain profiles and diurnal variations observed with TRMM

PR over the equatorial area. *Geophys. Res. Lett.*, **29**, 1584, doi:10.1029/2001GL014113.

Trilaksono, N. J., S. Otsuka, S. Yoden, K. Saito, and S. Hayashi, 2011: Dependence of model-simulated heavy rainfall on the horizontal resolution during the Jakarta Flood event in January–February 2007. *SOLA*, **7**, 193–196.

Trilaksono, N. J., S. Otsuka, and S. Yoden, 2012: A time-lagged ensemble simulation on the modulation of precipitation over West Java in January–February 2007. *Mon. Wea. Rev.*, **140**, 601–616.

Wallace, J. M., 1975: Diurnal variations in precipitation and thunderstorm frequency over the conterminous United States. *Mon. Wea. Rev.*, **103**, 406–419.

Wu, P., J. Hamada, S. Mori, Y. I. Tauhid, M. D. Yamanaka, and F. Kimura, 2003: Diurnal variation of precipitable water over a mountainous area of Sumatra Island. *J. Appl. Meteor.*, **42**, 1107–1115.

Wu, P., M. Hara, H. Fudeyasu, M. D. Yamanaka, J. Matsumoto, F. Syamsudin, R. Sulistyowati, and Y. S. Djajadihardja, 2007: The impact of trans-equatorial monsoon flow on the formation of repeated torrential rains over Java Island. *SOLA*, **3**, 93–96.

Yabu, S., S. Murai, and H. Kitagawa, 2005: Clear-sky radiation scheme. *NPD Rep.*, **51**, Japan Meteorological Agency, 53–64 (in Japanese).

Zumberge, J. F., M. B. Heflin, D. C. Jefferson, M. M. Watkins, and F. H. Webb, 1997: Precise point positioning for the efficient and robust analysis of GPS data from large networks. *J. Geophys. Res.*, **102**, 5005–5017.